scientific reports

Check for updates

OPEN

Lactoferrin targeting INTL1 receptor inhibits hepatocellular carcinoma progression via apoptosis and cell cycle signaling pathways

Abdulkadir Cidem[1,2], Gary Ro-Lin Chang[1], Chih-Ching Yen[3], Ming-Shan Chen[4], Shang-Hsun Yang[5] & Chuan-Mu Chen[1,6,7]✉

Hepatocellular carcinoma (HCC) constitutes 90% of liver cancer cases and ranks as the third leading cause of cancer-related mortality, necessitating urgent development of alternative therapies. Lactoferrin (LF), a natural iron-binding glycoprotein with reported anticancer effects, is investigated for its potential in liver cancer treatment, an area with limited existing studies. This study focuses on evaluating LF's anti-liver cancer effects on HCC cells and assessing the preventive efficacy of oral LF administration in a murine model. Data showed that LF exerted anti-proliferative effects on HepG2, Hep3B, and SK-Hep1 cells while having no cytotoxicity on healthy liver cells (FL83B). Mechanistically, LF induces mitochondrial-mediated apoptosis and G0/G1 cell cycle arrest in HepG2 cells, associated with increased phosphorylation of p38 MAPK and JNK for apoptosis, and ERK phosphorylation for cell cycle arrest. Intelectin-1 (INTL1) is identified as the receptor facilitating LF endocytosis in HepG2 cells, and downregulation of INTL1 inhibits LF-induced signaling pathways. Notably, oral LF administration prevents HCC development in nude mice with orthotopic HepG2 cell injection. This study unveils the mechanistic basis of LF action in HepG2 cells, showcasing its potential in HCC prevention. Importantly, we report the novel identification of INTL1 as the LF receptor in HepG2 cells, providing valuable insights for future exploration of LF and its derivatives in liver cancer therapy.

Keywords Hepatocellular carcinoma (HCC), Lactoferrin (LF), Apoptosis, Cell cycle arrest, Intelectin-1 (INTL1), Mitogen-activated protein kinase (MAPK)

Liver cancer remains a major health problem due to its increasing incidence, and hepatocellular carcinoma (HCC) accounts for approximately 90% of liver cancer cases and is listed as the third leading cause of cancer-related deaths[1]. Although substantial progress has been made in the study of HCC treatments, only approximately 20% of patients obtain access to them, and mortality rates are still high in many countries[2]. Epidemiological studies have shown that alcohol consumption, nonalcoholic fatty liver disease (NAFLD), and chronic hepatitis B virus (HBV), HCV, and human immunodeficiency virus (HIV) infections are important risk factors for fibrosis and HCC[3]. In the early stages, hepatectomy and local therapy are important treatment modalities, and HCC patients treated with these methods have a survival rate of over 50%. In the advanced stages of the disease, no effective treatment exists, and patients have a very poor prognosis[4]. Currently, chemotherapy is one of the most commonly used methods of cancer treatment. However, this method may have various side effects due to patient resistance that substantially affect quality of life[5].

[1]Department of Life Sciences, College of Life Sciences, National Chung Hsing University, Kuo Kuang Rd., Taichung 402, Taiwan. [2]Department of Molecular Biology and Genetics, Erzurum Technical University, Erzurum 25250, Turkey. [3]Department of Internal Medicine, China Medical University Hospital, College of Health Care, China Medical University, Taichung 404, Taiwan. [4]Department of Anesthesiology, Ditmanson Medical Foundation Chia-Yi Christian Hospital, Chia-Yi 600, Taiwan. [5]Department of Physiology, Institute of Basic Medical Sciences, National Cheng Kung University, Tainan 70101, Taiwan. [6]The iEGG and Animal Biotechnology Center, and Rong Hsing Research Center for Translational Medicine, National Chung Hsing University, Taichung 402, Taiwan. [7]Center for General Educational, National Quemoy University, Kinmen 892, Taiwan. ✉email: chchen1@dragon.nchu.edu.tw

Lactoferrin (LF) is a natural iron-binding glycoprotein (approximately 80 kD) that is largely secreted from the mammary gland tissues during an animal's lactating period, and nearly 5 g/L of LF is present in colostrum[6]. LF is also secreted in mucosal fluids, such as saliva, tears, bile, pancreatic juice, gastric juice, bronchial, and uterine secretions, and is also released from the secondary granules of neutrophils during inflammation[7,8]. In addition to acting as an iron-binding protein to regulate iron homeostasis and hematopoiesis, LF and LF-derived peptides also function as mediators linking innate and adaptive immune responses to exert antimicrobial, anti-inflammatory, anticancer, and neuroprotective effects, as well as promote bone health and wound healing[7–9]. In the liver tissue of mice, LF is taken up by endothelial and Kupffer cells[10], and oral administration of LF has been shown to exert liver protection by alleviating chemical-[11–13] and ethanol-induced liver injuries in mice[14,15]. Clinically, LF exerts anti-HCV effects in patients with chronic hepatitis[16,17]. Furthermore, the anticancer effects of LF have been extensively investigated in different human cancer cells, but related studies on the application of LF to treat HCC and the underlying molecular mechanisms remain limited. HepG2 is a human liver cancer cell line that is commonly used in studies of drug metabolism and hepatotoxicity. In this study, we aimed to assess the anti-liver cancer effects of bovine LF using a HepG2 cell model and a nude mouse xenograft model and to explore the membrane receptor for LF and the underlying signal transduction.

Results

LF exerts cytotoxic effects on human liver cancer cells

To assess the specific cytotoxic effects of LF on liver cancer cells, HepG2, Hep3B, and SK-Hep1 cells were tested, and the results were compared to those of the healthy mouse liver cell line FL83B (Fig. 1 and Supplementary Fig. S1). The LF treatments caused considerable inhibition of HepG2 cell proliferation but not healthy mouse FL83B liver cell proliferation (Fig. 1A). Moreover, LF also caused similar inhibitory effects on Hep3B and SK-Hep1 cell proliferation (Supplementary Fig. S1A). The LF-induced cytotoxic effects displayed a dose-dependent trend in these cancer cells, especially at concentrations of 5 and 10 mg/ml, which completely inhibited the proliferation of HepG2 and Hep3B cells (Fig. 1B and Supplementary Fig. S1B). Our results demonstrated that lactoferrin had no significant impact on normal liver cells, even at high doses such as 5 mg/ml and 10 mg/ml, while these doses effectively inhibited cell viability and growth in HCC cell lines (HepG2, Hep3B, and SK-Hep1). According to the European Food Safety Authority (EFSA), estimated daily intakes can reach up to 3.4 g for adults, with fortified products and energy bars containing as much as 4,000 mg/100 g[18]. Accordingly, the half maximal inhibitory concentration (IC_{50}) of LF for HepG2 cells was estimated at 5 mg/ml. Moreover, the LF treatments significantly inhibited the growth of HepG2 and Hep3B cell colonies after an extended incubation time, both in terms of colony size and number (Fig. 1C and Supplementary Fig. S1C).

LF promotes apoptosis in HepG2 cells

To further examine the LF-induced cytotoxic effects on HepG2 cells, a general apoptosis assay using Annexin V-FITC and PI labeling was performed (Fig. 2). In contrast to the DPBS-treated HepG2 cells, the LF treatments significantly increased HepG2 cell apoptosis, with over 20% apoptotic cells at 10 mg/ml of LF (Fig. 2A, B). The LF-induced necrosis remained at a relatively lower level (~3%) and was independent of LF concentrations. The intrinsic pathway of cell apoptosis is known to involve the breakdown of mitochondria and the release of proteins (e.g., cytochrome C) from the intermembrane space of mitochondria. To further examine the impact of LF treatment on the mitochondrial functionality of HepG2 cells, a TMRE-labeled mitochondrial membrane potential assay was performed. As indicated, functional mitochondria in live DPBS-treated HepG2 cells were labeled with red fluorescent TMRE dye; however, the fluorescent intensities decreased remarkably in LF-treated HepG2 cells in both dose- and time-dependent manners, with an approximately 40% decrease in the numbers of TMRE-labeled HepG2 cells when 5 and 10 mg/ml of LF were added (Fig. 2C–E). The results of Western blotting demonstrated that LF treatments decreased Bcl-2 protein levels while having no effect on Bax protein levels, leading to a substantially decreased intracellular Bcl-2/Bax ratio (Fig. 2F). Furthermore, the phosphorylation of the c-Jun protein and the release of cytochrome C were enhanced by LF treatment (Fig. 2F). Moreover, the cleavage of caspase 3 and poly (ADP-ribose) polymerase 1 (PARP1) proteins was also increased in the presence of LF (Fig. 2F). The changes in these apoptosis-associated marker proteins corresponded to the increase in LF-induced cell apoptosis and apoptosis-mediated mitochondrial damage in HepG2 cells.

LF induces apoptosis through p38 MAPK and JNK activation

MAPK pathways in the cell are known to direct extracellular stimuli from a receptor to the DNA in the nucleus to trigger the transcription of responsive genes[19]. Therefore, we first examined the effects of LF treatments on the expression of three classical MAPK pathways, including p38 MAPK, c-Jun N-terminal kinase (JNK), and extracellular signal-regulated kinases 1 and 2 (ERK1/2). Notably, the phosphorylation of p38 MAPK, JNK, and ERK was strongly activated by LF, showing a dose- and time-dependent trend (Fig. 3A, B). Moreover, LF was shown to be recognized in the protein lysates of HepG2 cells (Fig. 3A). Because p38 MAPK and JNK signal activation have been shown to induce apoptosis in a variety of cancer cells in response to chemotherapeutic agents[19], we further examined the effects of LF on HepG2 cells by pretreating cells with either 10 μM SB203580 (a p38 inhibitor) or 15 μM SP600125 (a JNK inhibitor) for 3 h, followed by 5 mg/ml LF treatment for 48 h (Fig. 3C–G). In this experiment, HepG2 cells showed approximately 72% and 66% viability after LF treatment in the presence of SB203580 and SP600125, respectively, compared to 57% viability in the absence of any inhibitors, demonstrating that neither SB203580 nor SP600125 can completely block the inhibitory effects of LF on HepG2 growth (Fig. 3C, D). However, the combination of SB203580 and SP600125 did not exhibit additive effects on HepG2 viability as predicted, which may be due to nonspecific cell death in the presence of a high inhibitor concentration. Consistently, the results of flow cytometry demonstrated that both SB203580 and SP600125 partially inhibited apoptosis in LF-treated HepG2 cells, but no additive effects were observed from

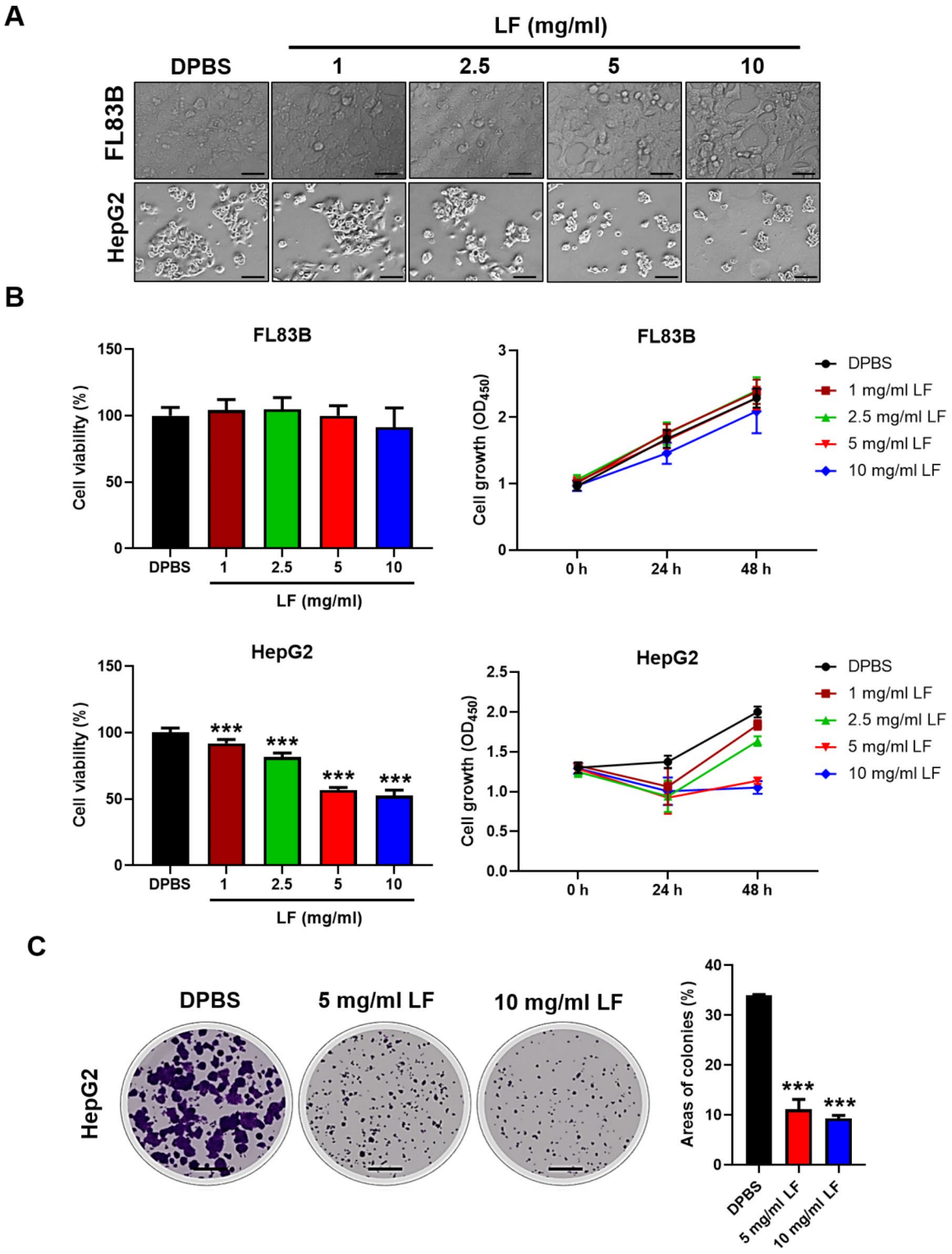

Fig. 1. Effects of LF on the proliferation of human liver cancer cells. (**A**) Representative images of HepG2 and FL83B cells after 48 h of incubation with either LF (1, 2.5, 5, and 10 mg/ml) or DPBS (control). (**B**) Cell viability and proliferation profiles. The cell viability (48 h) and proliferation profiles (0, 24, and 48 h) were tested by CCK-8. (**C**) Representative images of the HepG2 colony formation assay (scale bars, 500 μm). Statistical significance: * ($p < 0.05$), ** ($p < 0.01$), and *** ($p < 0.001$) vs. DPBS.

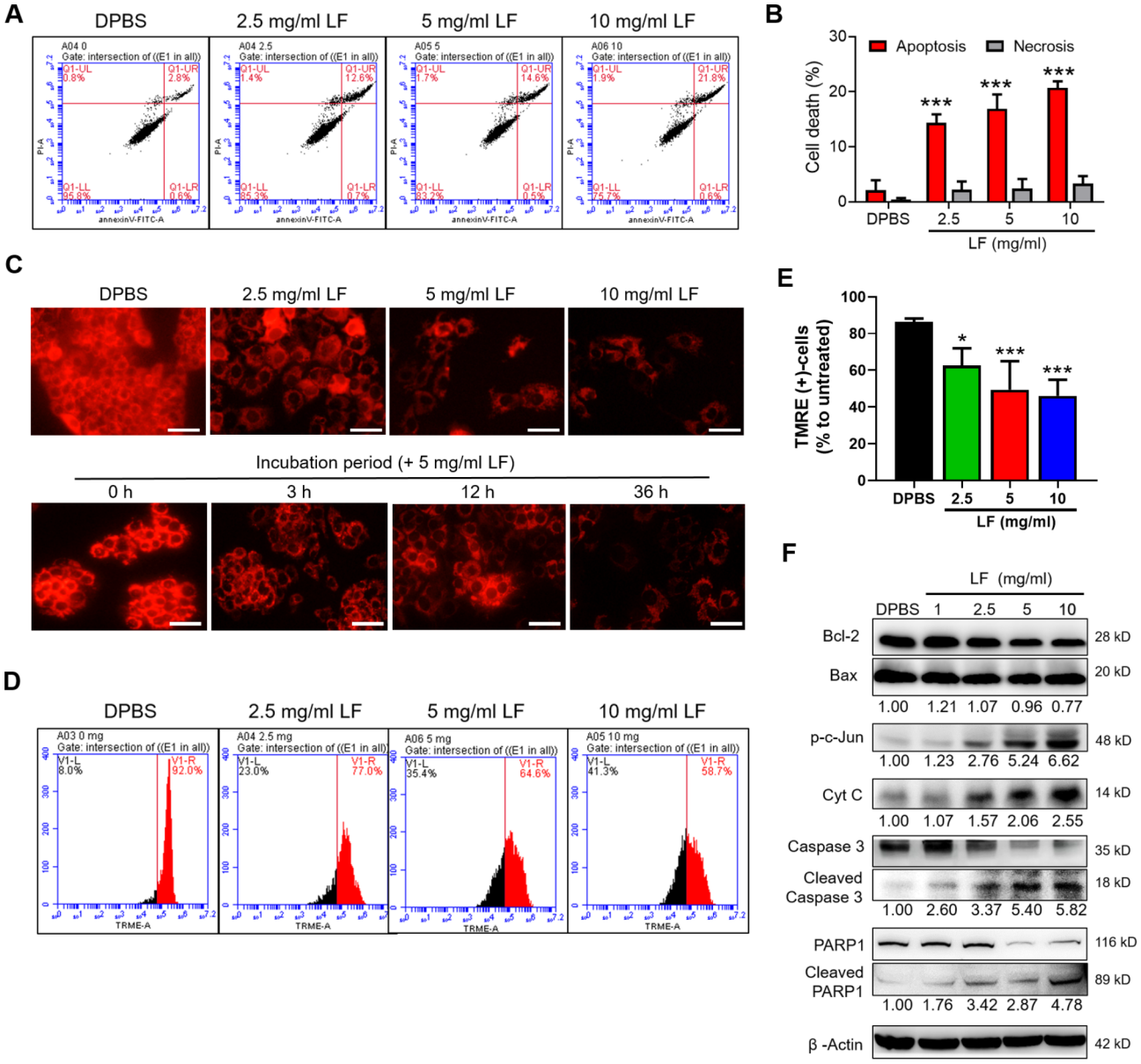

Fig. 2. LF induces mitochondrial-mediated apoptosis in HepG2 cells. (**A**) Representative flow cytometric analysis of apoptosis. After being exposed to LF for 48 h, HepG2 cells were stained with Annexin V-FITC antibodies and PI and then subjected to apoptotic analysis using flow cytometry. (**B**) The proportions of apoptotic and necrotic HepG2 cells after LF treatment. (**C**) Representative fluorescence images of the mitochondrial membrane potential assay. In this experiment, HepG2 cells with normal mitochondrial membrane potential were labeled with TMRE (red fluorescence). Scale bars, 50 μm. (**D**) Representative flow cytometric analysis of TMRE-labeled HepG2 cells. (**E**) The proportion of TMRE-positive HepG2 cells in the mitochondrial membrane potential assay using flow cytometry. (**F**) Western blot analysis of apoptosis-related proteins. The relative protein levels are shown below the representative images, which were determined after normalization and comparison with the DPBS-treated HepG2 lysates. Statistical significance: * ($p < 0.05$), ** ($p < 0.01$), and *** ($p < 0.001$) vs. DPBS.

the combination of the two inhibitors (Fig. 3E, F). The results of Western blotting demonstrated the specificities of SB203580 and SP600125 on the inhibition of p38 MAPK and JNK phosphorylation, respectively (Fig. 3G). Notably, SB203580 significantly reduced LF-induced cytochrome C release, but SP600125 did not. Moreover, SP600125 increased LF-induced p38 MAPK phosphorylation regardless of the presence of SB203580 (Fig. 3G). The combined results demonstrated that the p38 MAPK and JNK pathways are involved in LF-induced HepG2 apoptosis.

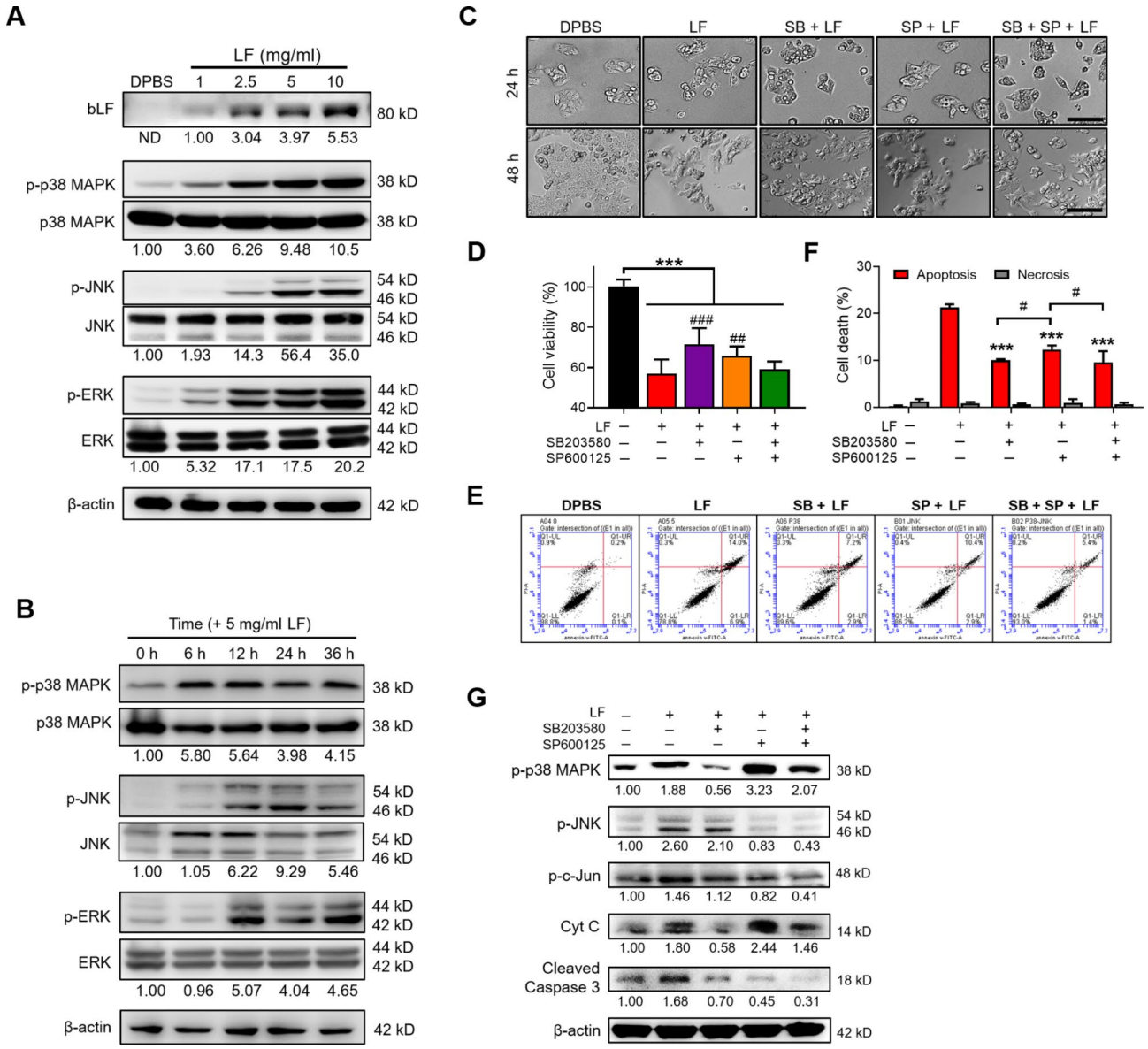

Fig. 3. LF induces cell apoptosis through the activation of p38 MAPK and JNK signaling. (**A**) Western blot images showing the entry of LF and the effects of LF treatment for 48 h on p38 MAPK, JNK, and ERK phosphorylation. The relative phosphorylated profiles shown below were determined by normalizing the phosphorylated protein intensity to the unphosphorylated protein intensity and comparing them with the DPBS-treated HepG2 lysates. ND means that the band intensity was not detectable. (**B**) Western blot images showing the time-course of p38 MAPK, JNK, and ERK phosphorylation after 5 mg/ml LF treatment. (**C**) Representative cell images at 24 and 48 h after treatment with LF (5 mg/ml) and inhibitors against p38 MAPK (SB203580) and JNK (SP600125). Scale bars, 100 μm. (**D**) Cell viability after treatment with LF and inhibitors (*, vs. no LF; #, vs. LF/no inhibitors). (**E**) Representative apoptosis analysis after treatment with LF and inhibitors. (**F**) The proportions of apoptotic and necrotic HepG2 cells after treatments with LF and inhibitors (*, vs. LF/no inhibitors). (**G**) Western blot images showing the changes in p38 MAPK and JNK phosphorylation and the release of cytochrome C and cleaved caspase 3 after treatment with LF and inhibitors. The relative protein levels were determined after β-actin normalization. Statistical significance: * ($p < 0.05$), ** ($p < 0.01$), and *** ($p < 0.001$); # ($p < 0.05$), ## ($p < 0.01$), and ### ($p < 0.001$).

LF arrests the HepG2 cell cycle at the G0/G1 phase via ERK-mediated upregulation of p21, p27, and p53

Since LF inhibited the proliferation of HepG2 cells in the present study, we next further examined its impact on HepG2 cell cycle progression. Apparently, the proportion of HepG2 cells in the G0/G1 phase dose-dependently increased after LF treatment compared to DPBS treatment, accompanied by decrease in the proportion of cells in the synthesis (S) and G2 phases, showing that LF induces cell cycle arrest at the G0/G1 phase (Fig. 4A, B). The results of Western blotting demonstrated that the tumor protein P53 (p53) and two inhibitor proteins of the

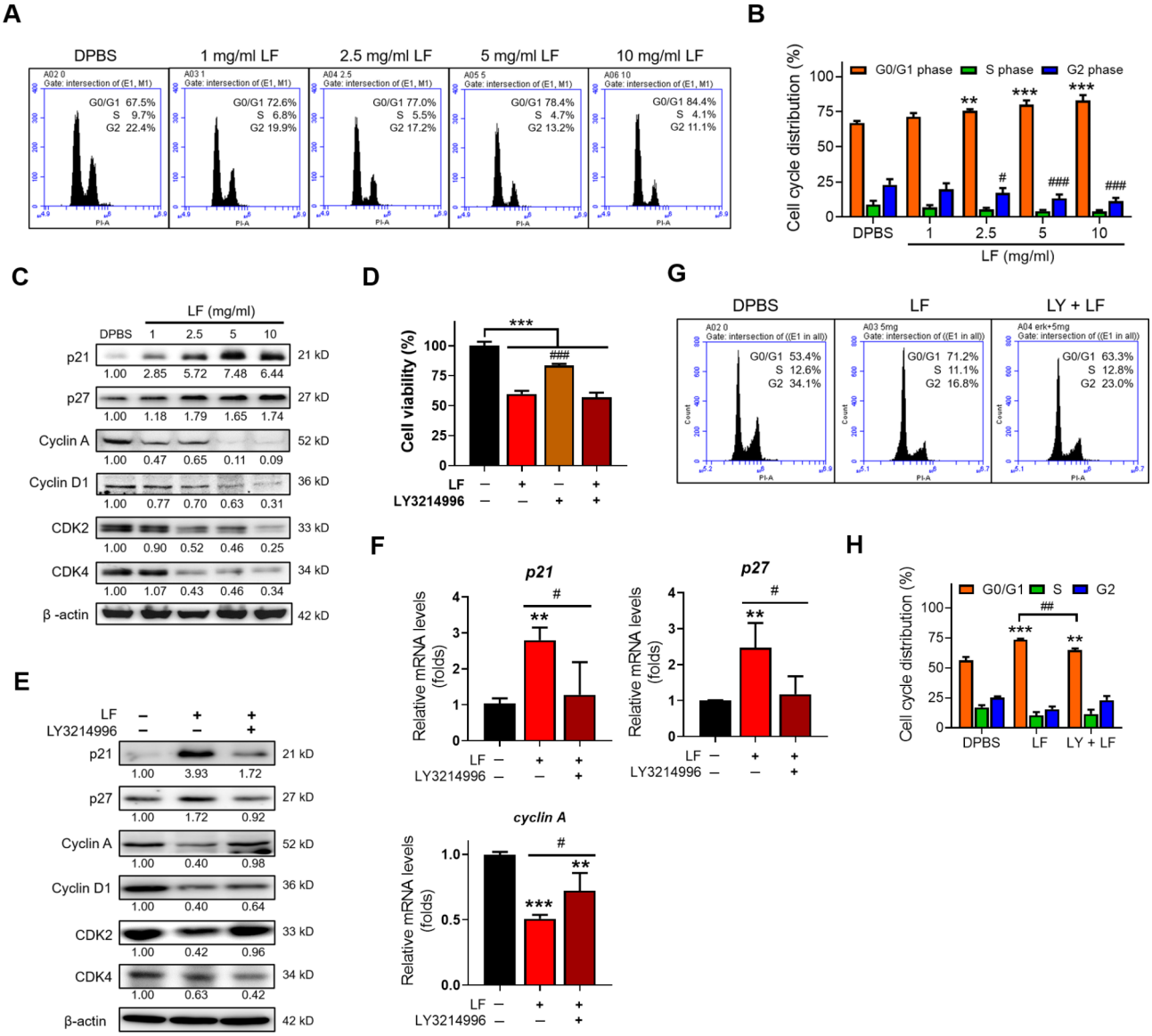

Fig. 4. LF arrests the HepG2 cell cycle at the G0/G1 phase through the activation of ERK signaling. (**A**) Representative flow cytometric analysis of the HepG2 cell cycle. (**B**) The proportions of HepG2 cells at different phases of the cell cycle (*, vs. G0/G1 phase/DPBS; #, vs. G2 phase/DPBS). (**C**) Western blot analysis of cell cycle-related proteins. The relative protein levels were determined after β-actin normalization. (**D**) Cell viability after treatment with LF and ERK inhibitor (LY3214996) (# vs. LF/no inhibitor). (**E**) Western blot images showing the changes in cell cycle-related proteins after treatments with LF and LY3214996. (**F**) Quantitative RT-PCR analysis showing the changes in p21, p27, and Cyclin A mRNA levels after treatments with LF and LY3214996 (*, vs. no LF). (**G**) Representative cell cycle analysis after treatment with LF and LY3214996. (**H**) Changes in the cell cycle distribution after treatment with LF and LY3214996 (*, vs. G0/G1 phase/DPBS). Statistical significance: * ($p < 0.05$), ** ($p < 0.01$), and *** ($p < 0.001$); # ($p < 0.05$), ## ($p < 0.01$), and ### ($p < 0.001$).

cell cycle, p21 and p27, were upregulated, while the related cyclins (cyclin A, cyclin D1) and cyclin-dependent kinases (CDK2, CDK4) that control the checkpoints of the cell cycle were downregulated by LF treatment (Fig. 4C). The literature reports that ERK activation is the key mechanism connecting external stimuli to induce and activate cell cycle events that control the transition from G1 to S phase[20] and thus is generally thought to promote cell proliferation. This notion seems to contradict our findings that LF promotes ERK phosphorylation and G0/G1 cell cycle arrest. To further verify the effects of LF on ERK activation and the results of G0/G1 cell cycle arrest, HepG2 cells were pretreated with 10 nM LY3214996 (an ERK inhibitor) for 3 h and then further treated with 5 mg/ml LF for an additional 48 h (Fig. 4D–H). The addition of LY3214996 dramatically reduced HepG2 viability in the absence of LF, showing that ERK activity is required for cell cycle progression. However, the addition of LY3214996 did not affect HepG2 viability in the presence of LF (Fig. 4D). However, LY3214996 reversed LF-induced p21, p27, and p53 upregulation, as well as LF-induced cyclin A, cyclin D1, and CDK2

downregulation, but the expression of CDK4 was further inhibited by the addition of LY3214996 (Fig. 4E, F). Furthermore, cell cycle analysis demonstrated that LY3214996 diminished LF-induced G0/G1 cell cycle arrest (Fig. 4G, H). These results suggested that LF induced ERK-mediated p21, p27, and p53 upregulation to arrest the HepG2 cell cycle at the G0/G1 phase.

INTL1 mediates LF-induced MAPK activation in HepG2 cells

The receptors for LF have been previously identified and include low-density lipoprotein receptor-related protein 1 (LRP1)[21], intelectin-1 (INTL1)[22,23], and Toll-like receptor 4 (TLR4)[24]. We next characterized their expression and determined which receptor mediates the LF-induced actions in HepG2 cells (Fig. 5). The results of Western blotting demonstrated that all of these receptors were detectable in HepG2 lysates. The LF-associated membrane proteins were next harvested through Co-IP with anti-LF antibodies, showing that LF interacted with INTL1 and LRP1 but did not interact with TLR4 (Fig. 5A). Moreover, using antibodies against tumor necrosis factor (TNF) receptor associated factor-2 (TRAF2), we found that TRAF2 also complexed with LF (Fig. 5A). To clarify whether LRP1 and INTL1 are involved in downstream MAPK activation, shRNA-mediated RNAi was conducted. Compared to infection with a control virus particle (NC), infection with sh-LRP1 lentivirus particles effectively inhibited LRP1 expression in HepG2 cells, but LF-induced downstream p38 MAPK, JNK, and ERK phosphorylation was not affected by LRP1 downregulation (Fig. 5B). Furthermore, transfection with sh-INTL1 plasmid DNA also confirmed its effectiveness in inhibiting INTL1 expression, and the downregulation of INTL1 in turn suppressed the entry of LF and LF-induced p38 MAPK, JNK, and ERK phosphorylation (Fig. 5C).

Oral administration of LF shows anti-liver cancer effects on mice

An in vivo study was conducted by injecting HepG2 cells into the livers of nude mice and orally administering either PBS (mock) or LF (100 or 200 mg/kg/day) for 30 days to evaluate the preventive effects on the development of HCC (Fig. 6). The mean body weight of the mice in the mock group continued to decrease throughout the course of oral administration, losing approximately 17% overall at the end; however, the mean body weight in the LF-Low group increased by approximately 7%, while that of the LF-High group was slightly decreased by nearly 5% (Fig. 6A). After one month, tumors were widely distributed in the livers of mock group mice, but the tumor distribution was markedly reduced in the LF-treated nude mice (Fig. 6B). The mean liver weight and the ratio of liver to body weight were markedly increased in the mock group compared to the two LF-treated groups, but no substantial difference was observed between the LF-Low and LF-High groups (Fig. 6C). H&E staining results showed that in the liver sections of the mock group, the tumor area and the border with the surrounding normal tissue were clearly visible, but they were difficult to identify in the liver sections of the LF treatment groups (Fig. 6D). Tumor markers, including vascular endothelial growth factor (VEGF) and cluster of differentiation

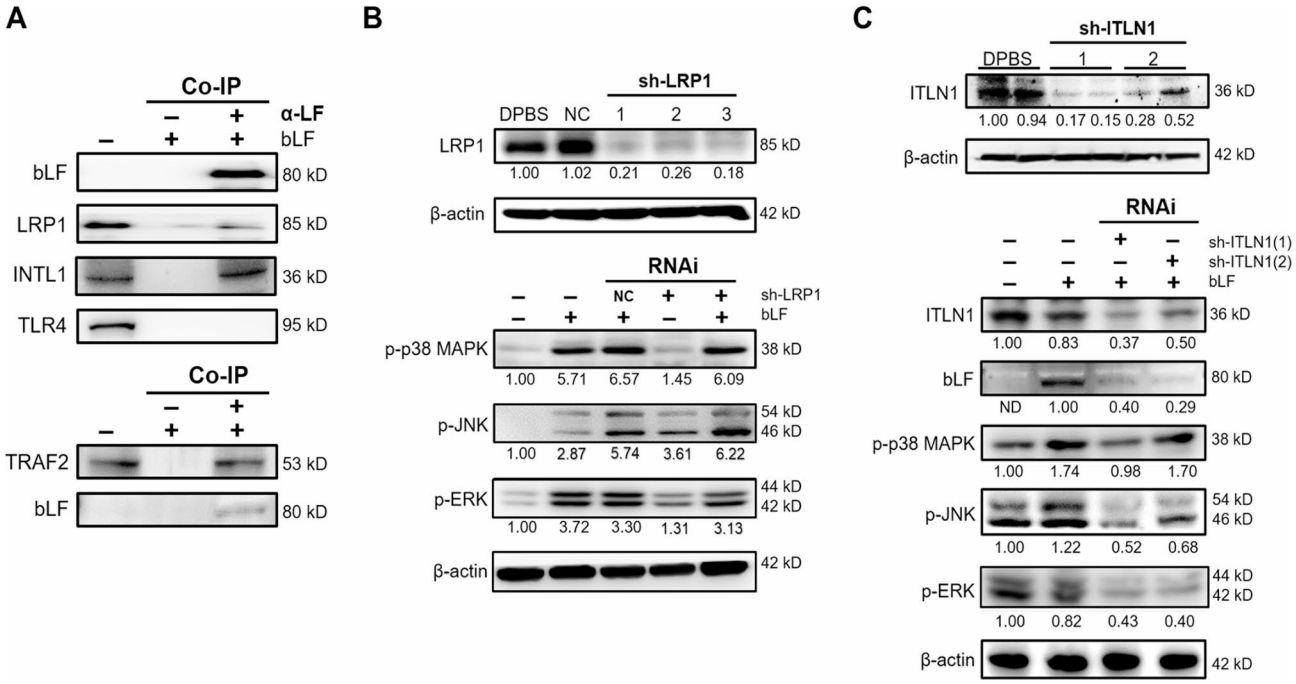

Fig. 5. INTL1 is the receptor for LF binding in HepG2 cells. (**A**) Western blot images showing the interactions of LF and the known receptors (LRP1, INTL1, and TLR4) for LF (upper, anti-LF) and the interaction of LF and TRAF2 (lower, anti-TRAF2) by Co-IP. (**B**) Western blot images showing the downregulation of LRP1 by LRP1-specific shRNAs (sh-LRP1) and the effects of LRP1 downregulation on p38 MAPK, JNK, and ERK phosphorylation. (**C**) Western blot images showing the downregulation of INTL1 by INTL1-specific shRNAs (sh-INTL1) and the effects of INTL1 downregulation on p38 MAPK, JNK, and ERK phosphorylation. The relative protein levels were determined after β-actin normalization.

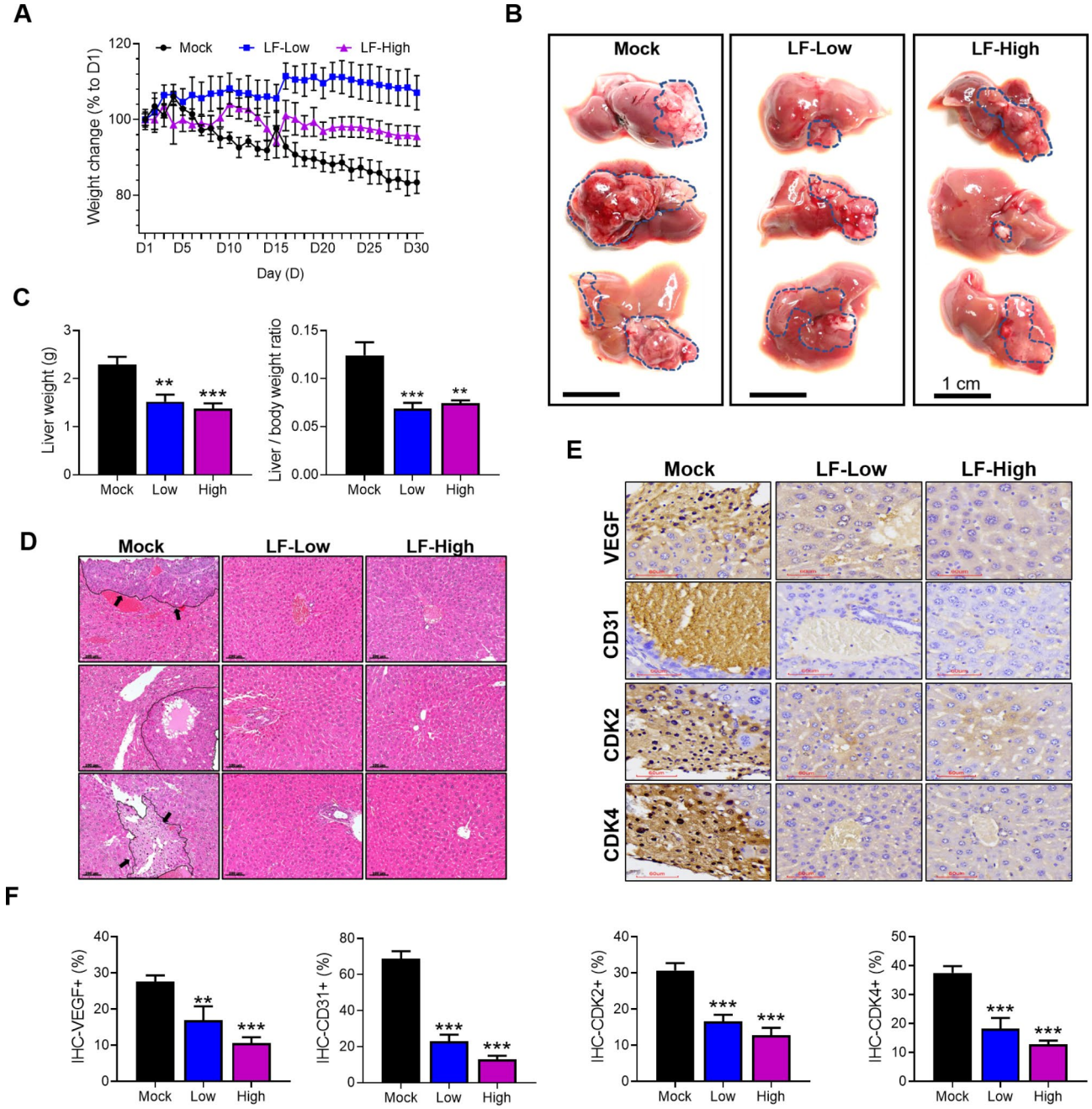

Fig. 6. LF exerts anti-HCC effects on mice. (**A**) Changes in mouse body weight during oral administration of PBS (Mock), 100 mg/kg/day LF (LF-Low), or 200 mg/kg/day LF (LF-High). (**B**) The appearance of the whole liver at the end of oral administration (each $n=3$). (**C**) Comparison of liver weight and the liver-to-body weight ratio. (**D**) H & E staining images of liver tissue sections (each $n=3$). Scale bars, 100 μm. Tumor areas in the mock group are marked with lines and indicated by arrows. (**E**) IHC staining images of VEGF, CD31, CDK2, and CDK4. The present images were photographed in the areas where a tumor was located (each $n=3$). (**F**) The positively stained areas for VEGF, CDK4, CDK2, and CD31 were quantified using ImageJ software. Statistical significance: * ($p<0.05$), ** ($p<0.01$), and *** ($p<0.001$) vs. mock.

31 (CD31), were largely present in the sections of the mock group according to the IHC staining, but they were significantly scaled down in both LF-treated groups (Fig. 6E, F). Similarly, the expression of CDK2 and CDK4 was upregulated in the mock group, in contrast to downregulated expression in the LF-treated groups (Fig. 6E, F). There were no statistically significant differences between the low-dose and high-dose LF treatment groups.

Discussion

HCC is one of the most difficult cancers to cure in modern medicine, and finding available alternative medications is still a challenging topic in cancer treatment research. Numerous anti-HCC natural compounds

extracted from herbal plants have been demonstrated to have pharmacological effects such as arresting the cell cycle and inhibiting apoptosis, autophagy, migration, and invasion while demonstrating a low toxicity on healthy cells[25]. In addition to these natural herbal compounds, LF is a natural iron-binding glycoprotein in milk that had been shown to exert anticancer effects in an earlier phase I trial[26] and is currently gaining increased attention for its potential application in the treatment of different cancers, such as oral cancer[27], prostate cancer[28], breast cancer[29], colon cancer[30], and lung cancer[31]. Numerous studies have revealed the protective effects of LF on chemical- and ethanol-induced liver injuries[11–15], but studies on the protective effects of LF on liver cancers are limited. In a previous study, Li et al. showed that LF inhibited the growth of HepG2 cells and other human cancer cells (A549, HT29, MDA231-LM2) via the induction of cell apoptosis[32]. Nevertheless, the involved receptors for LF and the underlying signal transduction in HepG2 cells have not been characterized. The present study demonstrated the growth-inhibitory effects of LF on HepG2 cells and two other human liver cancer cell lines, Hep3B and SK-Hep1 (Fig. 1 and Supplementary Fig. S1). The IC_{50} of LF is estimated at 5 mg/ml in our study, lower than the 20 g/L used in the study of Li et al.[32]. After considering the different mechanisms by which LF may exert its effects on different cell lines, HepG2 cells were selected as a model for further elucidating LF-induced tumor-toxic effects and the underlying signal transduction.

Several findings were reported in the present study. First, LF increases the apoptotic rate of HepG2 cells via the p38 MAPK and JNK pathways (Figs. 2 and 3). Induction of cell apoptosis is the most common mechanism through which many antitumor or anticancer agents exert their effects. Apoptosis is a highly regulated process that is initiated through either the intrinsic or extrinsic pathways. Intrinsic apoptosis is initiated by intracellular stress, leading to an imbalance between Bcl-2 anti-apoptotic protein levels and Bax pro-apoptotic protein levels, followed by the release of cytochrome C into the cytoplasm after mitochondrial membrane disturbance and the activation of downstream executioner caspases such as caspases 3, 6, and 7, which eventually cause cell death[33]. These events occurred in the HepG2 cells that had been exposed to LF, demonstrating that LF promotes mitochondria-mediated apoptosis in HepG2 cells. Furthermore, we found that LF increased the phosphorylation of c-Jun protein, implying the involvement of the JNK pathway. In fact, LF not only increased JNK phosphorylation but also promoted the phosphorylation of p38 MAPK and ERK in our study, showing the complexity of LF-induced signal transduction involved in the apoptosis of HepG2 cells. The activation of MAPK pathway-related proteins, such as p38 and ERK, is typically associated with cell survival and treatment resistance, though their roles can vary depending on the cellular context. However, in certain conditions, sustained activation of the p38 and ERK MAPK pathways has been shown to induce apoptosis and cell cycle arrest. For instance, studies by Qiang et al.[34] and Zhang et al.[35] demonstrated that p38/ERK MAPK signaling could promote apoptosis and cell cycle arrest in various cell lines, including HepG2 cells. Among these MAPKs, the activation of ERK is generally beneficial to the proliferation of cancer cells[36], which seems to be in conflict with the promotion of apoptosis by LF, which we will discuss later. To further verify the importance of p38 MAPK and JNK activation in HepG2 apoptosis, p38- (SB203580) and JNK-specific (SP600125) inhibitors were used. The introduction of a single inhibitor specifically inhibited the phosphorylation of p38 MAPK or JNK and reversed the effects of LF on HepG2 viability and apoptosis. The combination of p38 and JNK inhibitors did not increase cell viability or decrease the proportion of apoptotic cells, as predicted, suggesting that other signaling pathways were involved. It is worth noting that the application of SP600125 increased p38 MAPK phosphorylation in the absence or presence of the p38 inhibitor SB203580 (Fig. 3H). Both inhibitors decreased the cleavage of caspase 3, but only the p38 inhibitor inhibited cytochrome C release. This finding indicated that p38 MAPK mediates LF-induced apoptosis through the intrinsic pathway. The death receptor-mediated extrinsic pathway cannot be excluded in the present study because p38 MAPK and JNK activation have also been reported to trigger the extrinsic apoptotic pathway[37]. LF-induced MAPK activation has also been reported in bone, where its effects result in the proliferation of osteoblasts and the apoptosis of osteoclasts, showing another mechanism by which LF exerts beneficial effects on bone health[38].

Second, LF induces ERK activation and the upregulation of p21, p27, and p53 to cause cell cycle arrest at G0/G1 phase in HepG2 cells (Fig. 4). Disturbing the checkpoints leading to cell cycle arrest is another strategy that anticancer agents use to restrict tumor growth and cancer development. In this study, LF treatment was found to arrest the HepG2 cell cycle at G0/G1 phase, as demonstrated by the downregulation of the related cyclins (cyclin A and cyclin D1) and CDKs (CDK2 and CDK4), as well as the upregulation of two inhibitor proteins, p21 and p27. A similar cycle arrest profile was reported in MDA-MB-231 cells (breast cancer) after exposure to human LF, where the cell cycle was arrested at the G1 to S transition phase, accompanied by a remarkable decrease in the expression levels of CDK2, CDK4, and cyclin E and an increase in the expression levels of p21[39]. The upregulation of p21 and p27 is frequently reported in cancer cells after exposure to anticancer agents (e.g., histone deacetylase (HDAC) inhibitors[40] and simvastatin[41]). The literature indicates that the accumulation of p21 and p27 inhibits cyclin E/CDK2 and cyclin D/CDK4 complex formation, which in turn prevents the progression of cancer cells from G1 to S phase[42]. In this study, ERK activation was thought to mediate downstream p21 and p27 upregulation due to the finding that LF-induced cell cycle arrest and the inhibition of cyclin A, cyclin D1, and CDK2 were restored by LY3214996, an ERK inhibitor. Moreover, LY3214996 inhibited LF-induced upregulation of p21 and p27. Similar ERK activation-induced cell cycle arrest has also been reported in prostate cancer cells treated with bisphenol[43]. p53 is a central tumor suppressor that is often inactivated in many tumor types. We found that LF upregulated p53 expression in HepG2 cells, while LF-induced p53 upregulation was inhibited in the presence of LY3214996, suggesting that p53 is downstream of the ERK pathway. A recent genome-wide study by Engeland et al. reported that nearly half of all genes transcriptionally regulated by p53 are repressed, including a variety of cell cycle regulators[44]. They demonstrated that p53 upregulates p21 expression, and then p21 blocks several cyclin/CDK complexes by activating p21/retinoblastoma protein (RB) signaling. In addition, the activation of p21/RB signaling also upregulates p27 expression to block the cyclin A/E/CDK2 complex[44]. ERK has dual and opposing effects because numerous studies have shown that ERK activation increases oncogenic

cell proliferation; however, many compounds (e.g., icaritin[45], quercetin[46], simvastatin[47], etc.) have been reported to induce ERK activation-dependent apoptosis[20]. In this regard, p53 has been reported to induce apoptosis through the activation of p38 MAPK[48] and JNK[49], suggesting that p53 is also downstream of p38 MAPK- and JNK-mediated pathways and that p53 mediates the crosstalk between LF-induced cell cycle arrest and apoptosis.

Third, INTL1 mediates LF-induced MAPK activation in HepG2 cells (Fig. 5). The finding that intact LF was present in HepG2 lysates proved that LF enters the cytoplasm via endocytosis. To date, LRP1, INTL1, and TLR4 have been identified as LF receptors[21–24], but only LRP1 and INTL1 were shown for the first time to bind LF in HepG2 cells. We next showed that INTL1 knockdown prevented LF entry and the phosphorylation of p38 MAPK, JNK, and ERK, indicating that INTL1 acts as a LF receptor that aids in downstream MAPK activation in HepG2 cells. INTL1 is a galactofuranose-specific lectin that exists in the lipid raft on the brush border of enterocytes[50], where it can mediate the uptake of LF with high specificity through an endocytic mechanism and affect the subcellular localization and subsequent release of LF to the apical side of enterocytes[22,23]. According to the study of Akiyama et al.[23], LF associated with cell surface INTL1 undergoes endocytosis, localizes with early endosome antigen 1 (EEA1), and remains intact for a certain period of time. LRP1 is a low-specificity receptor for LF in contrast to INTL1, and we found that LF-induced MAPK activation in HepG2 cells was independent of LRP1. Nonetheless, other LRP1-induced signaling pathways cannot be fully excluded. It is interesting to note the association of TRAF2 with LF and INTL1. TRAF2 is an intracellular adaptor protein that interacts with at least 100 proteins and is involved in various cancer-relevant processes, including the activation of various MAPK cascades and the control of apoptosis[51]. TRAF2 can function as a tumor suppressor or as a tumor promoter depending on the conditions. Recently, Liang et al. reported that TRAF2 is upregulated in both human liver cancer cell lines (HepG2, Huh7, Hep3B, etc.) and tissues, and high TRAF2 expression is linked to a poor prognosis of HCC patients[52]. However, further studies are required to determine whether TRAF2 is involved in LF/INTL1-mediated MAPK activation and the downstream cellular responses.

Fourth, oral administration of LF exerts anti-liver cancer effects on mice (Fig. 6). At present, there are limited in vivo studies evaluating the efficacy of LF against liver cancers. Previously, Woodfield et al.[53] developed an orthotopic mouse model to create an animal xenograft, surgically implanting HepG2 and Huh-6 cells into the right or left liver lobes via a midline abdominal incision. In the present study, we injected HepG2 cells into the liver of each nude mouse to evaluate the effects of oral LF administration on the development of HCC. Our data proved that oral LF administration moderates weight loss during treatment and prevents the development of HCC to a significant extent. The IHC images showed that LF downregulated VEGF and CD31 expression in the liver, suggesting that LF inhibits angiogenesis during HCC development. Moreover, the downregulation of CDK2 and CDK4 expression in the LF-treated nude mice was supportive of the fact that LF arrests the HepG2 cell cycle. Similar LF-induced antiangiogenic effects have been reported in lung tumorigenesis in our previous human VEGF-overexpressing transgenic mouse model[31]. Recently, Ayuningtyas et al. used oral cancer mouse models to demonstrate that LF can be endocytosed through LRP1 and bound to endogenous TRAF6 to inhibit the NFκB pathway, which explains the LF-mediated cellular responses against tumor angiogenesis[54]. Despite state-of-the-art techniques being continuously developed to improve the LF-mediated effects on various cancer types[55], more in-depth investigations remain necessary to provide a satisfactory prognosis for clinical application.

Summarily, LF bound to the membrane INTL1 receptor, initiated its entry by endocytosis, and then activated the p38 MAPK and JNK pathways to promote HepG2 apoptosis through the intrinsic pathway. Moreover, LF endocytosed through the INTL1 receptor also activated the ERK pathway to upregulate p21, p27, and p53 expression, which in turn downregulated downstream cyclins and CDKs to arrest the HepG2 cell cycle at G0/G1 phase (Fig. 7). In this study, p53 may mediate the crosstalk between LF-induced apoptosis and cell cycle arrest, and LF binding to INTL1 may recruit TRAF2 to the formed endosomes, but the function of TRAF2 recruitment requires further characterization. In addition, the results of the animal experiment demonstrated that oral LF administration prevents HCC development, which is consistent with our findings in HepG2 cell cultures. To our knowledge, these results are reported for the first time.

Conclusions

The present study illustrates the potential of LF against hepatocellular carcinoma from both cell- and animal-based experiments. The identification of INTL1 as the receptor for LF binding and the underlying signal transduction in HepG2 cells offer novel insights for HCC treatment with LF or LF-derived peptides.

Methods

Chemicals, kits, and cell culture media

Bovine lactoferrin (LF) with a purity > 98% was supplied by Phermpep Co., Ltd. (Taichung, Taiwan). A stock LF solution (250 mg/ml) was prepared in phosphate-buffered saline (PBS) and stored at -20 °C until use. Modified Eagle's medium (MEM), Dulbecco's modified Eagle's medium (DMEM), fetal bovine serum (FBS), 100× MEM-nonessential amino acid (MEM-NEAA) solution, 100 mM sodium pyruvate solution, 100× penicillin/streptomycin solution, and the BCA protein assay kit were purchased from Thermo Fisher Scientific Inc. (Waltham, MA, USA). Cell Counting Kit-8 (CCK-8) was purchased from MedChemExpress (Monmouth Junction, NJ, USA). Propidium iodide (PI)/RNase staining buffer was purchased from BD Pharmingen (San Diego, CA, USA). A mitochondrial membrane potential assay kit was purchased from Cell Signaling Technology (Danvers, MA, USA). An Annexin V-FITC/PI apoptosis detection kit was purchased from Elabscience Biotechnology (Wuhan, China). The Presto™ DNA/RNA/protein extraction kit was purchased from Geneaid Biotech Ltd. (Taipei, Taiwan). The MMLV Reverse Transcription Kit and 2× qPCRBIO SyGreen Mix were purchased from Protech Technology Enterprise Co., Ltd. (Taipei, Taiwan). The Novolink™ Polymer Detection System was purchased from Leica Biosystems (Deer Park, IL, USA). Inhibitors for p38 MAPK (SB203580) and

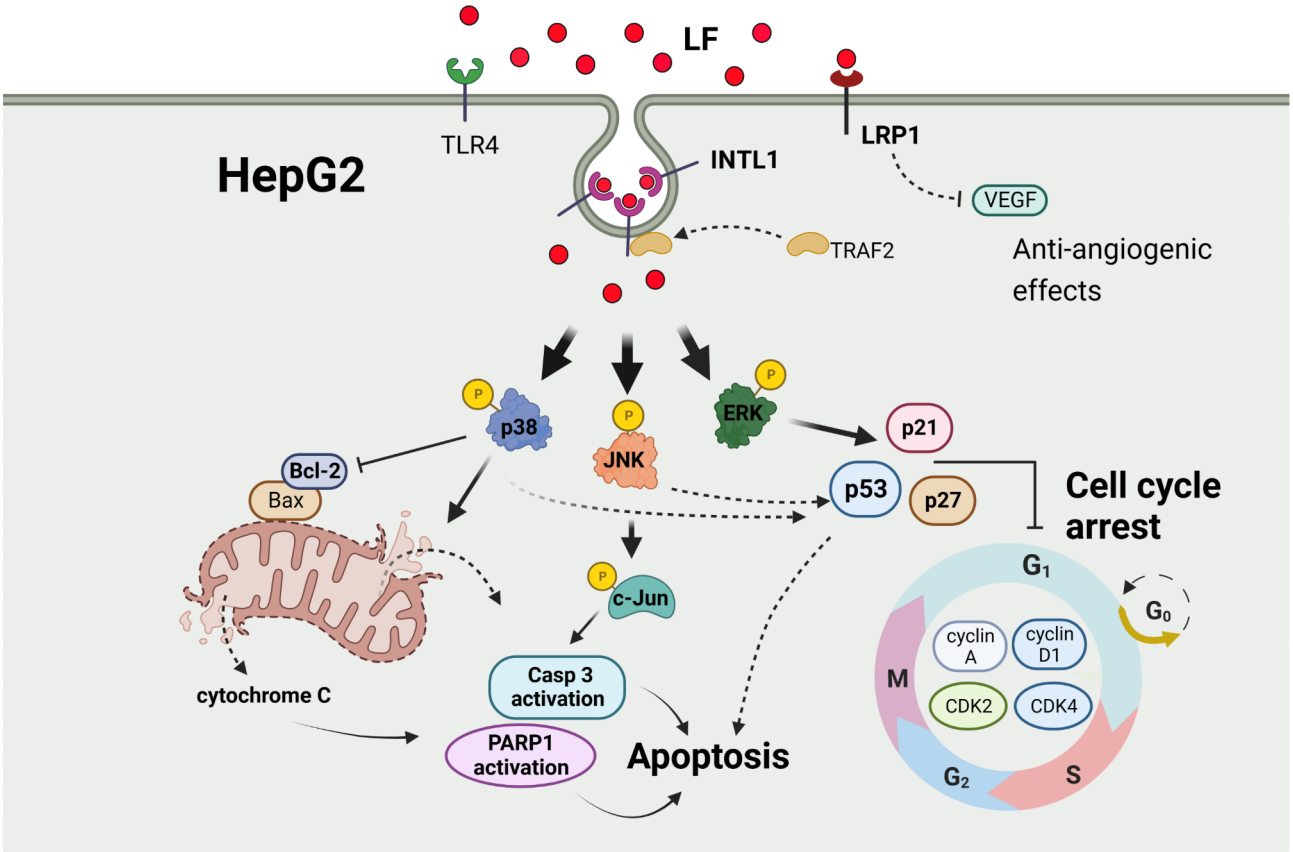

Fig. 7. The proposed mechanism that illustrates the effects of LF on HepG2 cells. →: promotion; T: inhibition; dashed lines: hypothesized actions.

JNK (SP600125) were purchased from Merck (Darmstadt, Germany). ERK inhibitor (LY3214996) was purchased from Cayman Chemical (Ann Arbor, MI, USA).

Cell culture

The cell lines used in this study, including FL83B (normal liver cells), HepG2 (hepatocellular carcinoma), Hep3B (hepatocellular carcinoma), and SK-Hep1 (liver adenocarcinoma), were purchased from the Bioresource Collection and Research Center (BCRC), Hsinchu, Taiwan. FL83B cells were maintained in DMEM supplemented with 10% FBS, 1% MEM-NEAA, 1 mM sodium pyruvate, and 1% penicillin/streptomycin. HepG2, Hep3B, and SK-Hep1 cells were maintained in MEM supplemented with 10% FBS, 1% MEM-NEAA, 1 mM sodium pyruvate, and 1% penicillin/streptomycin. All of the cultures were incubated at 37 °C in a humidified atmosphere of 5% CO_2.

Cell viability assay

Cell viability was determined using a CCK-8 kit. Briefly, cells were seeded in 96-well plates (3000 cells/well) and treated with different concentrations of LF (1, 2.5, 5, and 10 mg/ml) or an equal volume of DPBS as a control. At the indicated time points (0, 24, and 48 h), the old media was replaced with new media, and 10 µl of CCK-8 solution was subsequently added. After 2 h of incubation at 37 °C, the absorbance at 450 nm was measured using a microplate spectrophotometer.

Colony formation assay

Cells were seeded in 6-well plates (500 cells/well) and allowed to grow in the presence of LF (5 and 10 mg/ml) or not (using PBS as a control). The incubation persisted for 9 days, and the media were refreshed every 3 days until the end of the incubation. Afterward, the cells were washed with PBS and then stained with 0.1% crystal violet for 15 min. Images were acquired using a Lionheart FX automated microscope (BioTek Instruments, Winooski, VT, USA), and the surface areas of the cell colonies were measured using ImageJ software.

Apoptosis analysis

For apoptosis analysis, cells were grown in 6-well plates at an initial cell density of 10^6 cells per well for 24 h and then treated with different concentrations of LF for another 48 h. The same procedures were also applied to the other cell experiments presented in this study. Apoptosis analysis was performed using an Annexin V-FITC/PI apoptosis detection kit. Briefly, the collected HepG2 cells were washed twice with cold PBS and resuspended in

binding buffer (10 mM HEPES, 140 mM NaCl, 2.5 mM $CaCl_2$, pH 7.4) at a cell density of nearly 10^6 cells per ml. Aliquots of the cell suspension (100 µl) were then mixed with Annexin V-FITC antibody (20-fold dilution) and PI (50 µg/ml) and incubated for 30 min at room temperature under light protection. Afterward, the sample volume was brought up to 500 µl with binding buffer, followed by analysis using a BD Accuri C6 Plus flow cytometer.

Mitochondrial membrane potential assay

A mitochondrial membrane potential assay kit was used to assess changes in mitochondrial membrane potential. This assay was performed by incubating an adequate number of LF-treated cells in a tetramethylrhodamine (TMRE, 200 mM) labeling solution at 37 °C for 20 min. Cells were harvested, washed three times with ice-cold PBS, and then analyzed by flow cytometry. For microscopic observation, cells were grown on 18-mm sterile coverslips (5000 cells/slip) and treated with the same procedures as described above. The fluorescence intensities of TMRE (650–690 nm) were evaluated by cellSens imaging software (Olympus).

Cell cycle analysis

For the cell cycle analysis, the collected HepG2 cells were washed with ice-cold PBS, fixed with 70% ethanol for 2 h, and finally resuspended in PI/RNase staining buffer at a cell density of nearly 10^6 cells per ml. After incubation at 37 °C for 30 min, samples were subjected to cell cycle analysis using a BD Accuri C6 Plus flow cytometer (BD Biosciences, Mountain View, CA, USA).

Western blot analysis

The preparation of protein lysates and the related procedures for Western blot analysis were performed as previously described[56]. Briefly, protein lysates were prepared by lysing cells in 1× RIPA buffer containing protease and phosphatase inhibitors. The total protein concentration was determined using a BCA protein assay kit. Samples of 35 µg total protein were loaded, separated by SDS-PAGE, and then transferred to PVDF membranes. The PVDF membranes were then sequentially treated by blocking (5 min), primary antibody incubation (4 °C, overnight), TBS-T wash (10 min, 3 times), secondary antibody incubation (10000-fold dilution, 2 h), TBS-T wash (10 min, 3 times), and detection of chemical luminescence immediately. Appropriate dilutions of the primary antibodies used in this study are listed in Supplementary Table S1.

RNA isolation and quantitative real-time PCR (qRT–PCR)

Total RNA was extracted using a Presto™ DNA/RNA/Protein Extraction Kit according to the manufacturer's instructions. Two micrograms of total RNA from each sample was transcribed into cDNA using an MMLV Reverse Transcription Kit. qRT-PCR was performed by mixing an aliquot of cDNA sample with target gene primers and 2× qPCRBIO SyGreen Mix in a total volume of 20 µl, followed by PCR running using the QuantStudio™ 6 Pro Real-Time PCR System (Applied Biosystems, Waltham, MA, USA). The primers used in this study are listed as follows: p21, 5'-CGATGGAACTTCGACTTTGTCA-3' and 5'-CACAAGGGTACAAGACAG TG-3'; p27, 5'-CCGGTGGACCACGAAGAGT-3' and 5'-GCTCGCCTCTTCCATGTCTC-3'; Cyclin A, 5'-GCC ATTAGTTTACCTGGACCCAGA-3' and 5'-ACTGACATGGAAGACAGGAACCT-3'.

Coimmunoprecipitation (Co-IP)

The harvested HepG2 cells were resuspended in lysis buffer (20 mM Tris-HCl, 137 mM NaCl, 1% Triton X-100, 2 mM EDTA, pH 8.0) at 4 °C. The cell suspensions were then centrifuged (12,000 × *g*, 15 min) to collect the supernatants. Antibodies targeting the protein of interest were added and allowed to incubate at 4 °C overnight. Protein G magnetic beads (Cytiva 28-9440-08, Merck) were then introduced to the protein mixtures and incubated for 1 h at 4 °C with gentle mixing. Afterward, the beads were washed with lysis buffer to remove any nonspecifically bound proteins. Finally, proteins bound to beads were eluted with 50 µl of elution buffer (100 mM Tris-HCl, 4% SDS, 0.2% bromophenol blue, 20% glycerol). The samples were subjected to Western blot analysis after heating at 50 °C for 10 min.

RNA interference (RNAi)

The shRNA lentivirus particles targeting LRP1 (sh-LRP1) and lentivirus particles used for control (NC), as well as shRNA plasmid clones targeting INTL1 (sh-INTL1), were obtained from the RNA Technology Platform and Gene Manipulation Core, Academia Sinica, Taipei, Taiwan (http://rnai.genmed.sinica.edu.tw). shRNA-related information is presented in Supplementary Table S2.

For sh-LRP1 lentivirus transduction, cells were cultured in 6-well plates to a confluency of 70 - 80%, followed by the addition of sh-LRP1 lentivirus particles at an MOI (multiplicity of infection) of 5 and incubation for 24 h at 37 °C in a humidified incubator. The media were refreshed with puromycin (2 µg/ml)-containing media every 3 days until puromycin-resistant colonies formed. The resistant cell colonies were selected and expanded, and the efficiency of LRP1 knockdown was determined by Western blot analysis.

For the transfection of sh-INTL1 plasmids, cells were cultured in 6-well plates to a confluency of 70–80%, followed by transfection with a TransIT-X2 dynamic delivery system (Mirus Bio LLC., Madison, WI, USA) based on the recommended conditions. The efficiency of INTL1 knockdown was determined by Western blotting after 48 h of transfection.

Orthotopic mouse experiment

In vivo studies were performed in nude mice (BALB/c, male, 4–5 weeks old, 18–22 g) that were obtained from the National Laboratory Animal Center, Taipei, Taiwan. Procedures such as housing and feeding were performed in

accordance with protocols approved by the Institutional Animal Care and Use Committee of National Chung Hsing University (IACUC No. 104 − 091). The study is reported in accordance with ARRIVE guidelines.

To generate tumors, 40 µl of HepG2 cells (approximately 1×10^6 cells) mixed with 60 µl of Matrigel matrix (Corning) were implanted into the right lobe of the liver through an abdominal incision. One week after injection, mice were randomly divided into three groups (each $n = 3$). Our previous study demonstrated that a dose of 900 mg/kg LF produced no significant side effects in mice[57]; however, to minimize potential side effects, we selected doses within the EFSA-specified safety range for bovine lactoferrin[18]. Based on this information, nude mice were treated with PBS (mock group), 100 mg/kg/day LF (low-dose group), and 200 mg/kg/day LF (high-dose group) for thirty days. During oral administration, mouse body weight was recorded. At the end of the treatment, the mice were anesthetized with inhaled isoflurane and sacrificed by cervical dislocation to collect tissue samples for further analysis. Liver samples were collected, which were either immediately frozen in liquid nitrogen and stored at -80 °C until further use or fixed in 10% neutral formalin for subsequent paraffin embedding and tissue section staining.

Immunohistochemistry (IHC) staining

The paraffin-embedded liver sections were cut at 5-µm thickness in glass slides and subjected to IHC staining using a Novolink™ Polymer Detection System according to the manufacturer's instructions. After dewaxing, liver sections on the slides were incubated in peroxidase-blocking buffer for 5 minutes to eliminate endogenous peroxidase activity. The slides were then incubated overnight at 4°C with primary antibody solutions (100-fold dilution) and subsequently incubated with HRP-conjugated secondary antibody solutions (500-fold dilution) for 2 h. After three PBS washes, 3,3'-diaminobenzidine (DAB) was added for color development. After being thoroughly washed with water, the slides were counterstained with hematoxylin, dehydrated, mounted, and observed under a microscope. The positively stained areas of IHC were quantitatively measured using ImageJ software.

Statistical analysis

All experiments were repeated independently at least three times. The data are presented as the mean ± SD and were plotted using GraphPad Prism 8.0 software (Boston, MA, USA). Statistical analyses were performed by one-way or two-way ANOVA with Tukey's multiple comparison. Statistical significance is marked by * ($^*p < 0.05$, $^{**}p < 0.01$, and $^{***}p < 0.001$) and # ($^{\#}p < 0.05$, $^{\#\#}p < 0.01$, and $^{\#\#\#}p < 0.001$).

Data availability

Data is provided within the manuscript or supplementary information files.

Received: 16 September 2024; Accepted: 5 December 2024
Published online: 28 December 2024

References

1. Llovet, J. M. et al. Hepatocellular carcinoma. *Nat. Rev. Dis. Primers*. **7** (1), 6 (2021).
2. Muzellec, L., Bourien, H. & Edeline, J. Patients' experience of systemic treatment of hepatocellular carcinoma: A review of the impact on quality of life. *Cancers* **14** (1), 179 (2021).
3. Kulik, L. & El-Serag, H. B. Epidemiology and management of hepatocellular carcinoma. *Gastroenterology* **156** (2), 477–491 (2019).
4. Pasini, F., Serenari, M., Cucchetti, A. & Ercolani, G. Treatment options for recurrence of hepatocellular carcinoma after surgical resection: Review of the literature and current recommendations for management. *Hepatoma Res.* **6**, 26 (2020).
5. Ikeda, M. et al. Chemotherapy for hepatocellular carcinoma: Current status and future perspectives. *Jpn J. Clin. Oncol.* **48** (2), 103–114 (2018).
6. Tsuji, S., Hirata, Y., Mukai, F. & Ohtagaki, S. Comparison of lactoferrin content in colostrum between different cattle breeds. *J. Dairy. Sci.* **73** (1), 125–128 (1990).
7. Artym, J. & Zimecki, M. Colostrum and lactoferrin protect against side effects of therapy with antibiotics, anti-inflammatory drugs and steroids, and psychophysical stress: A comprehensive review. *Biomedicines* **11** (4), 1015 (2023).
8. Superti, F. Lactoferrin from bovine milk: A protective companion for life. *Nutrients* **12** (9), 2562 (2020).
9. Arias, M. et al. Anticancer activities of bovine and human lactoferricin-derived peptides. *Biochem. Cell. Biol.* **95** (1), 91–98 (2017).
10. Courtoy, P. J., Moguilevsky, N., Retegui, L. A., Castracane, C. E. & Masson, P. L. Uptake of lactoferrin by the liver. II. Endocytosis by sinusoidal cells. *Lab. Invest.* **50** (3), 329–334 (1984).
11. Tung, Y. T. et al. Lactoferrin protects against chemical-induced rat liver fibrosis by inhibiting stellate cell activation. *J. Dairy. Sci.* **97** (6), 3281–3291 (2014).
12. Yin, H. et al. Lactoferrin protects against acetaminophen-induced liver injury in mice. *Hepatology* **51** (3), 1007–1016 (2010).
13. Yin, H., Cheng, L., Agarwal, C., Agarwal, R. & Ju, C. Lactoferrin protects against concanavalin A-induced liver injury in mice. *Liver Int.* **30** (4), 623–632 (2010).
14. Li, D. et al. Lactoferrin alleviates acute alcoholic liver injury by improving redox-stress response capacity in female C57BL/6J mice. *J. Agric. Food Chem.* **69** (49), 14856–14867 (2021).
15. Li, D. et al. Daily dose of bovine lactoferrin prevents ethanol-induced liver injury and death in male mice by regulating hepatic alcohol metabolism and modulating gut microbiota. *Mol. Nutr. Food Res.* **65** (18), e2100253 (2021).
16. Okada, S. et al. Dose-response trial of lactoferrin in patients with chronic hepatitis C. *Jpn J. Cancer Res.* **93** (9), 1063–1069 (2002).
17. Tanaka, K. et al. Lactoferrin inhibits hepatitis C virus viremia in patients with chronic hepatitis C: A pilot study. *Jpn J. Cancer Res.* **90** (4), 367–371 (1999).
18. European Food Safety Authority (EFSA). Scientific opinion on bovine lactoferrin. *EFSA J.* **10** (5), 2701 (2012).
19. Sui, X. et al. p38 and JNK MAPK pathways control the balance of apoptosis and autophagy in response to chemotherapeutic agents. *Cancer Lett.* **344** (2), 174–179 (2014).
20. Chambard, J. C., Lefloch, R., Pouysségur, J. & Lenormand, P. ERK implication in cell cycle regulation. *Biochim. Biophys. Acta*. **1773** (8), 1299–1310 (2007).
21. Willnow, T. E., Goldstein, J. L., Orth, K., Brown, M. S. & Herz, J. Low density lipoprotein receptor-related protein and gp330 bind similar ligands, including plasminogen activator-inhibitor complexes and lactoferrin, an inhibitor of chylomicron remnant clearance. *J. Biol. Chem.* **267** (36), 26172–26180 (1992).

22. Shin, K., Wakabayashi, H., Yamauchi, K., Yaeshima, T. & Iwatsuki, K. Recombinant human intelectin binds bovine lactoferrin and its peptides. *Biol. Pharm. Bull.* **31** (8), 1605–1608 (2008).
23. Akiyama, Y. et al. A lactoferrin-receptor, intelectin 1, affects uptake, sub-cellular localization and release of immunochemically detectable lactoferrin by intestinal epithelial Caco-2 cells. *J. Biochem.* **154** (5), 437–448 (2013).
24. Ando, K. et al. Human lactoferrin activates NF-kappaB through the toll-like receptor 4 pathway while it interferes with the lipopolysaccharide-stimulated TLR4 signaling. *FEBS J.* **277** (9), 2051–2266 (2010).
25. Zheng, Y. et al. Recent progress in understanding the action of natural compounds at novel therapeutic drug targets for the treatment of liver cancer. *Front. Oncol.* **11**, 795548 (2021).
26. Hayes, T. G. et al. Phase I trial of oral talactoferrin alfa in refractory solid tumors. *Invest. New. Drugs.* **24** (3), 233–240 (2006).
27. Sakai, T., Banno, Y., Kato, Y., Nozawa, Y. & Kawaguchi, M. Pepsin-digested bovine lactoferrin induces apoptotic cell death with JNK/SAPK activation in oral cancer cells. *J. Pharmacol. Sci.* **98** (1), 41–48 (2005).
28. Shankaranarayanan, J. S., Kanwar, J. R., Al-Juhaishi, A. J. & Kanwar, R. K. Doxorubicin conjugated to immunomodulatory anticancer lactoferrin displays improved cytotoxicity overcoming prostate cancer chemo resistance and inhibits tumour development in TRAMP mice. *Sci. Rep.* **6**, 32062 (2016).
29. Zhang, Y., Nicolau, A., Lima, C. F. & Rodrigues, L. R. Bovine lactoferrin induces cell cycle arrest and inhibits mTOR signaling in breast cancer cells. *Nutr. Cancer.* **66** (8), 1371–1385 (2014).
30. Li, H., Li, C., Zhang, B. & Jiang, H. Lactoferrin suppresses the progression of colon cancer under hyperglycemia by targeting WTAP/m(6)A/NT5DC3/HKDC1 axis. *J. Transl Med.* **21** (1), 156 (2023).
31. Tung, Y. T. et al. Bovine lactoferrin inhibits lung cancer growth through suppression of both inflammation and expression of vascular endothelial growth factor. *J. Dairy. Sci.* **96** (4), 2095–2106 (2013).
32. Li, H. Y. et al. Investigation and comparison of the anti-tumor activities of lactoferrin, alpha-lactalbumin, and beta-lactoglobulin in A549, HT29, HepG2, and MDA231-LM2 tumor models. *J. Dairy. Sci.* **102** (11), 9586–9597 (2019).
33. Kashyap, D., Garg, V. K. & Goel, N. Intrinsic and extrinsic pathways of apoptosis: Role in cancer development and prognosis. *Adv. Protein Chem. Struct. Biol.* **125**, 73–120 (2021).
34. Qiang, Y. et al. LukS-PV induces cell cycle arrest and apoptosis through p38/ERK MAPK signaling pathway in NSCLC cells. *Biochem. Biophys. Res. Commun.* **521** (4), 846–852 (2020).
35. Zhang, G. et al. β-Thujaplicin induces autophagic cell death, apoptosis, and cell cycle arrest through ROS-mediated akt and p38/ERK MAPK signaling in human hepatocellular carcinoma. *Cell. Death Dis.* **10** (4), 255 (2019).
36. Sugiura, R., Satoh, R. & Takasaki, T. ERK: A double-edged sword in cancer. ERK-dependent apoptosis as a potential therapeutic strategy for cancer. *Cells* **10** (10), 2509 (2021).
37. Ibraheem, K., Yhmed, A. M. A., Nasef, M. M. & Georgopoulos, N. T. TRAF3/p38-JNK signalling crosstalk with intracellular-TRAIL/Caspase-10-induced apoptosis accelerates ROS-driven cancer cell-specific death by CD40. *Cells* **11** (20), 3274 (2022).
38. Liu, M. et al. Lactoferrin promotes MC3T3-E1 osteoblast cells proliferation via MAPK signaling pathways. *Int. J. Biol. Macromol.* **107** (Pt A), 137–143 (2018).
39. Damiens, E. et al. Lactoferrin inhibits G1 cyclin-dependent kinases during growth arrest of human breast carcinoma cells. *J. Cell. Biochem.* **74** (3), 486–498 (1999).
40. Natarajan, U. et al. Cell cycle arrest and cytotoxic effects of SAHA and RG7388 mediated through p21(WAF1/CIP1) and p27(KIP1) in cancer cells. *Med. (Kaunas).* **55** (2), 30 (2019).
41. Wang, S. T., Ho, H. J., Lin, J. T., Shieh, J. J. & Wu, C. Y. Simvastatin-induced cell cycle arrest through inhibition of STAT3/SKP2 axis and activation of AMPK to promote p27 and p21 accumulation in hepatocellular carcinoma cells. *Cell. Death Dis.* **8** (2), e2626 (2017).
42. Bhoora, S. & Punchoo, R. Policing cancer: Vitamin D arrests the cell cycle. *Int. J. Mol. Sci.* **21** (23), 9296 (2020).
43. Bilancio, A. et al. Bisphenol A induces cell cycle arrest in primary and prostate cancer cells through EGFR/ERK/p53 signaling pathway activation. *Oncotarget* **8** (70), 115620–115631 (2017).
44. Engeland, K. Cell cycle regulation: p53-p21-RB signaling. *Cell. Death Differ.* **29** (5), 946–960 (2022).
45. Guo, Y., Zhang, X., Meng, J. & Wang, Z. Y. An anticancer agent icaritin induces sustained activation of the extracellular signal-regulated kinase (ERK) pathway and inhibits growth of breast cancer cells. *Eur. J. Pharmacol.* **658** (2–3), 114–122 (2011).
46. Kim, Y. H., Lee, D. H., Jeong, J. H., Guo, Z. S. & Lee, Y. J. Quercetin augments TRAIL-induced apoptotic death: Involvement of the ERK signal transduction pathway. *Biochem. Pharmacol.* **75** (10), 1946–1958 (2008).
47. Jang, H. J. et al. Statin induces apoptosis of human colon cancer cells and downregulation of insulin-like growth factor 1 receptor via proapoptotic ERK activation. *Oncol. Lett.* **12** (1), 250–256 (2016).
48. Dziegielewska, B., Brautigan, D. L., Larner, J. M. & Dziegielewski, J. T-type Ca2 + channel inhibition induces p53-dependent cell growth arrest and apoptosis through activation of p38-MAPK in colon cancer cells. *Mol. Cancer Res.* **12** (3), 348–358 (2014).
49. Kang, Y. J. et al. MHY2251, a new SIRT1 inhibitor, induces apoptosis via JNK/p53 pathway in HCT116 human colorectal cancer cells. *Biomol. Ther. (Seoul).* **31** (1), 73–81 (2023).
50. Wrackmeyer, U., Hansen, G. H., Seya, T. & Danielsen, E. M. Intelectin: A novel lipid raft-associated protein in the enterocyte brush border. *Biochemistry* **45** (30), 9188–9197 (2006).
51. Siegmund, D., Wagner, J. & Wajant, H. TNF receptor associated factor 2 (TRAF2) signaling in cancer. *Cancers (Basel).* **14** (16), 4055 (2022).
52. Liang, X. et al. The TRAF2-p62 axis promotes proliferation and survival of liver cancer by activating mTORC1 pathway. *Cell. Death Differ.* **30** (6), 1550–1562 (2023).
53. Woodfield, S. E. et al. A novel cell line based orthotopic xenograft mouse model that recapitulates human hepatoblastoma. *Sci. Rep.* **7** (1), 17751 (2017).
54. Ayuningtyas, N. F. et al. Bovine lactoferrin suppresses tumor angiogenesis through NF-kB pathway inhibition by binding to TRAF6. *Pharmaceutics* **15** (1), 165 (2023).
55. El-Fakharany, E. M., Abu-Serie, M. M., Ibrahim, A. & Eltarahony, M. Anticancer activity of lactoferrin-coated biosynthesized selenium nanoparticles for combating different human cancer cells via mediating apoptotic effects. *Sci. Rep.* **13** (1), 9579 (2023).
56. Chang, G. R. et al. Kefir peptides ameliorate osteoporosis in AKR1A1 knockout mice with vitamin C deficiency by promoting osteoblastogenesis and inhibiting osteoclastogenesis. *Biomed. Pharmacother.* **156**, 113859 (2022).
57. Pu, T. Y. et al. Lactoferrin as a therapeutic agent for attenuating hepatic stellate cell activation in thioacetamide-induced liver fibrosis. *Biomed. Pharmacother.* **174**, 116490 (2024).

Acknowledgements

We thank our colleague, Dr. Ying-Wei Lan, in the Molecular Embryology & DNA Methylation Laboratory, Department of Life Sciences, National Chung Hsing University, for interesting discussions and his help with technical issues.

Author contributions

S.H.Y. and C.M.C.: conceptualization and resources; A.C., G.R.L.C., C.C.Y. and M.S.C.: methodology, experiments and formal analysis; A.C., G.R.L.C. and S.H.Y.: data curation; A.C. and G.R.L.C.: writing—original draft

preparation; C.M.C.: writing—review and editing, visualization, supervision, funding acquisition; A.C.: project administration. All authors have read and agreed to the published version of the manuscript.

Funding
This research was funded by the grant MOST-110-2313-B-005-039-MY3 from the Ministry of Science and Technology of Taiwan (C.M.C.) and partially supported by the Higher Education Sprout Project from the Ministry of Education (MOE-113-S-0023-A) in Taiwan (C.M.C.).

Declarations

Competing interests
The authors declare no competing interests.

Ethical approval and consent to participate
All animal experiments were approved by the Institutional Animal Care and Use Committee of National Chung Hsing University (IACUC No. 104－091). Experimental protocols and animal care were provided according to the guideline for the care and use of animals established by National Chung Hsing University.

Consent for publication
All authors confirm their consent for publication the manuscript.

Additional information
Supplementary Information The online version contains supplementary material available at https://doi.org/10.1038/s41598-024-82514-4.

Correspondence and requests for materials should be addressed to C.-M.C.

Reprints and permissions information is available at www.nature.com/reprints.

Publisher's note Springer Nature remains neutral with regard to jurisdictional claims in published maps and institutional affiliations.